RSC Advances

PAPER

View Article Online
View Journal | View Issue

Cite this: *RSC Adv.*, 2022, **12**, 18102

Phase transition and electronic properties of Co–As binary compounds at high pressure †

Ao Zhang,[ab] Yaqian Dan,[a] Han Liu,[ab] Siyuan Liu,[c] Jincheng Yue,[a] Junda Li,[a] Yanping Huang,[a] Yanhui Liu*[a] and Tian Cui*[a]

Received 1st April 2022
Accepted 30th May 2022

DOI: 10.1039/d2ra02114e

rsc.li/rsc-advances

New stable stoichiometries in the Co–As system are investigated up to 100 GPa by the CALYPSO structure prediction method. In particular, we found three novel stable compounds of Co_2As-*Pnma*, $CoAs_2$-*Pnnm*, and $CoAs_3$-*C*2/*m* at high pressure. According to the theoretical electronic band structures, the structures of Co_2As-*Pnma*, $CoAs_2$-*Pnnm*, and $CoAs_3$-*C*2/*m* have metallic characters, and a pressure-induced electronic topological transition was found in $CoAs_3$-*C*2/*m*, which is not shown in other stoichiometries of the Co–As system. The calculated results of the electron localization function show that there are polar covalent bond interactions between Co atoms and As atoms in $CoAs_2$-*Pnnm* and $CoAs_3$-*C*2/*m*. The present results can be helpful for understanding diverse structures and properties of Co–As binary compounds under high pressure.

1 Introduction

With several decades of effort, great achievements have been made in the field of condensed-matter physics. However, materials with better properties under extreme conditions are still being sought and studied. High pressure can provide a good way to search for new materials with new crystal phases, nonconventional stoichiometry, and outstanding properties.[1–5] For instance, unexpected stable stoichiometry of some binary systems were predicted under pressure.[6,7] Furthermore, the pressure-induced electronic topological transition in the structure of IrP has been uncovered by Ma by first-principles calculations.[8] The study shows that pressure has a strong influence in tuning the electronic properties and can also enhance the properties of materials.[9–11]

Compared with main group V compounds, the arsenide has been focused and researched under pressure since it exhibits unique structural features. For example, the arsenide is an important member of topological superconductors. Pressure-induced topological superconducting phases are observed in Cd_3As_2 and $SrAs_3$.[12,13] A non-monotonic pressure dependence of thermal conductivity was noticed in BAs due to the pressure-induced competing responses of three-phonon and four-phonon interactions, which has never been predicted or experimentally observed for any other materials.[14,15] To the best of our knowledge, the Co–As system has rarely been reported under pressure. On the basis of the interesting properties of above arsenide, it is necessary to explore the structure characters and chemical bonding of the Co–As binary compounds under pressure.

In the present paper, by means of first-principles swarm-intelligence structure search, we explored the binary Co–As phase diagram at 0–100 GPa. The previously reported structures of Co_2As-$P\bar{6}2m$, CoAs-*Pnam*, $CoAs_2$-$P2_1/c$, and $CoAs_3$-$Im\bar{3}$ were successfully reproduced at ambient conditions. Furthermore, three novel stable compounds (Co_2As-*Pnma*, $CoAs_2$-*Pnnm*, and $CoAs_3$-*C*2/*m*) were predicted under high pressure. At the same time, the details of electronic properties exhibit different bonding characters in these compounds under pressure. Interestingly, pressure-induced electronic topology transitions in CoAs3-*C*2/*m* phase have been confirmed. Our result represents a significant step toward understanding structural and electrical behaviour of the binary Co–As system under extreme condition.

2 Computational methods

CALYPSO method is the swarm-intelligence based particle swarm optimization (PSO) algorithm,[16–18] on which we predicted Co–As binary compounds under pressure of 0–100 GPa. In the framework of density functional theory, the structural optimizations, electronic structure and phonon calculations were performed. The generalized gradient approximation Perdew–Burke–Ernzerhof (GGA-PBE)[19] was employed to treat exchange-correlation energy as implemented in the Vienna *ab initio* simulation package (VASP) code,[20] and projector-augmented-wave method[21] was employed for cobalt and arsenic with

[a]*Institute of High Pressure Physics, School of Physical Science and Technology, Ningbo University, Ningbo 315211, China. E-mail: liuyanhui@nbu.edu.cn; cuitian@nbu.edu.cn*

[b]*Department of Physics, College of Science, Yanbian University, Yanji 133000, China*

[c]*School of Physics, Southeast University, Nanjing 211189, China*

† Electronic supplementary information (ESI) available. See https://doi.org/10.1039/d2ra02114e

$3d^8 4s^1$ and $4s^2 4p^3$ as valence states, respectively. The cutoff energy of 800 eV and Monkhorst–Pack scheme with $2\pi \times 0.04$ $Å^{-1}$ were chosen to ensure that all of the enthalpy calculations were well converged to better than 1 meV per atom.[22,23] The full potential linearized augmented plane-wave approach developed in the WIEN2k package (Fig. S0†) is used to assess the correctness of the generalized gradient approximation Perdew–Burke–Ernzerhof utilized at high pressure.[24] The DFT + U method was used to evaluate the effect of the U value for the transition metal element Co(ESI Fig. 6. and ESI Table 2†), the result proved that U had less impact on the Co–As system. The chemical stability of the Co–As system is examined by using the *ab initio* molecular dynamics (AIMD) simulations in the constant-temperature and constant-volume ensemble. The temperature is controlled at 300 K. The time step is set as 1 fs and each simulation lasts 5 ps. We used electron localization function (ELF)[25] to investigate the bonding characteristics between atoms, and calculated phonons by supercell approach of PHONOPY program to determine dynamic stability of structure.[26,27]

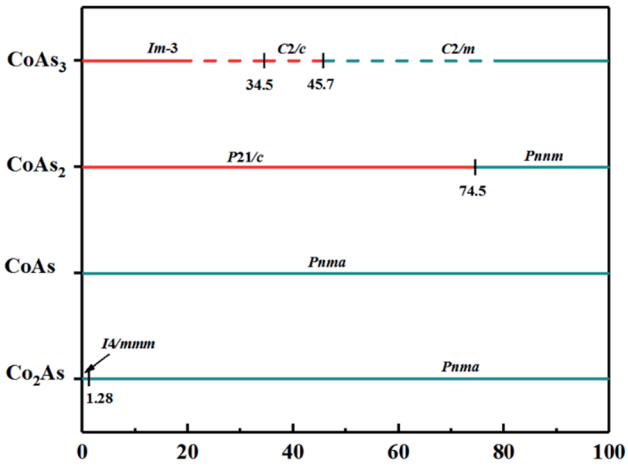

Fig. 2 Predicted pressure-composition phase diagram of Co–As crystal phases. Cyan and red colours represent the metallic and non-metallic phases, respectively. The solid (dash) lines represent stable (metastable) phases.

3 Results and discussion

3.1. Crystal structure

The variable-cell simulation with cell sizes of 1–4 formula units (f.u.) was performed structure prediction for $CoAs_x$ ($x = 1/2$; 1; 2; 3) at 0–100 GPa. We calculated the enthalpy of formation (ΔH_f) of each stoichiometric compound, as shown in Fig. 1, to study thermodynamic stability of predicted Co–As compounds. The relative thermodynamic stability of different Co–As compounds with respect to elemental solids Co and As is calculated according to following equation: $\Delta H_f(CoAs_x) = [H(CoAs_x) - H(Co) - xH(As)]/(x + 1)$. In the formula, H(M) represents the enthalpy of structure at corresponding pressure (M = $CoAs_x$, Co, As). In Fig. 1, solid star indicates thermodynamically stable phases and unstable or metastable phases are expressed by hollow star.

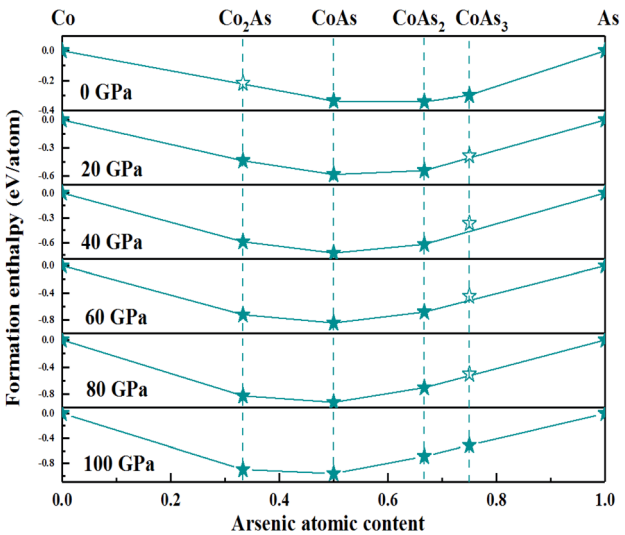

Fig. 1 Relative enthalpies of formation of Co–As phases with respect to elemental cobalt and arsenic solids. The convex hulls connecting stable phases (solid star) are shown by solid lines. Metastable phases are shown by open star.

The built pressure-composition phase diagram of the Co–As system is shown in Fig. 2, with stable structures identified using colours and space groups. The metallic and non-metallic phases are represented by cyan and red colours, respectively. As can be seen in the Fig. 2, all predicted stable structures are metal phase under pressure. The structural parameters and atomic coordinates of predicted structures are presented in Table 1. The predicted stable structures at ambient pressure are in good agreement with the experimental results,[28–31] validating the applicability to the Co–As system of our adopted structure searching method and PBE functional.

Pressure exhibits unique advantages in finding new materials,[32–36] thus the crystal structure and electron properties of these structures under high pressure will be examined in detail next. The full information of the initial pressure structures and phase diagrams of stable structures at different pressures are shown in ESI Fig. 1, 2, 3, and ESI Table 1,† respectively. The morphologies of predicted structures are presented in Fig. 3. The stoichiometric Co_2As has the lowest-enthalpy structure with $I4/mmm$, then at 1.28 GPa, it gives to the *Pnma* phase. Simultaneously, the distance between Co atoms and As atoms changes from 2.346 Å to 2.370 Å. Our calculation indicates that Co_2As-*Pnma* will be stable up until 100 GPa. Turning to CoAs, $CoAs_2$, and $CoAs_3$, Co atoms and As atoms in all predicted crystal structures form a Co–As octahedral environmental configuration, in which Co atoms occupy the center of the body and As atoms occupy the vertices. In the $CoAs_2$-*Pnnm*, there are As–As bonds with bond lengths is 2.292 Å. $CoAs_3$ is crystallized in a skutterudite-type structure at ambient pressure. The bond length of Co–As is 2.363 Å, and As atoms formed rectangular As_4 ring with As–As distances of 2.655 Å and 2.529 Å. Our calculations show that the cubic $CoAs_3$-$Im\bar{3}$ will be stabilized up to 34.5 GPa. With the increase of pressure, the structure changes from $Im\bar{3}$ phase to metastable $C2/c$ phase, and in the $C2/c$ phase,

Table 1 The lattice parameters and the Wyckoff position of predicted structures in the Co–As system

Space group pressure	Lattice parameters	Atomic coordinates (fractional)				Sites
Pnma-Co_2As 1.28 GPa	$a = 5.611$ Å	Co1	0.039	0.250	0.317	4c
	$b = 3.693$ Å	Co2	0.648	0.250	0.565	4c
	$c = 5.883$ Å	As1	0.739	0.250	0.882	4c
	$\alpha = \beta = \gamma = 90.0°$					
Pnnm-$CoAs_2$ 74.5 GPa	$a = 4.867$ Å	Co1	0.500	0.000	0.500	2c
	$b = 5.433$ Å	As1	0.823	0.139	1.000	4g
	$c = 2.636$ Å					
	$\alpha = \beta = \gamma = 90.0°$					
*C*2/*m*-$CoAs_3$ 45.7 GPa	$a = 8.882$ Å	Co1	0.176	0.000	0.923	4i
	$b = 4.348$ Å	As1	0.055	0.000	0.288	4i
	$c = 5.404$ Å	As2	0.108	0.500	0.851	4i
	$\alpha = \gamma = 90.0°$	As3	0.827	0.500	0.596	4i
	$\beta = 92.06°$					

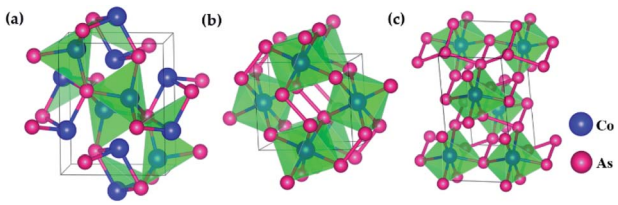

Fig. 3 Structures of predicted Co–As system for (a) Co_2As-*Pnma* at 1.28 GPa; (b) $CoAs_2$-*Pnnm* at 74.5 GPa, and (c) $CoAs_3$-*C*2/*m* at 45.7 GPa. The blue and pink spheres are Co atoms and As atoms, respectively.

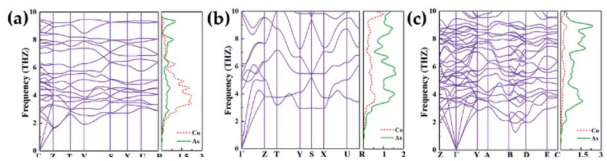

Fig. 4 Phonon dispersion relations and phonon density of states projected on Co atoms and As atoms for (a) Co_2As-*Pnma* at 1.28 GPa (b) $CoAs_2$-*Pnnm* at 74.5 GPa, and (c) $CoAs_3$-*C*2/*m* at 45.7 GPa.

the As atoms are in the form of chains with the distance of 2.359 Å, and the distance between Co atoms and As atoms turns into 2.242 Å. As pressure increases to 45.7 GPa, the structure changes to the *C*2/*m* phase, and distances between Co–As and As–As change to 2.286 Å and 2.510 Å, respectively. To judge their stability, the phonon dispersion curves for Co_2As-*Pnma*, $CoAs_2$-*Pnnm*, and $CoAs_3$–*C*2/*m* are calculated, as presented in Fig. 4. All above phases are dynamically stable in their accessible pressures since no imaginary vibrational modes are observed in the Brillouin zone.[37–41] To confirm the thermodynamic stability of the predicted structure, the AIMD at finite temperatures for Co_2As-*Pnma*, $CoAs_2$-*Pnnm*, and $CoAs_3$–*C*2/*m* are calculated, as presented in ESI Fig. 4.†[42,43]

3.2. Electronic properties

As shown in Fig. 5, we calculated band structures and the partial density of states (DOS) to investigate electronic properties of various Co–As compounds. Under high pressure, predicted structures exhibit metallic feature by evidence of overlap between conduction bands and valence bands at the Fermi level. In the structures of Co_2As-*Pnma*, the majority of the occupied states come from Co-d states near Fermi level (Fig. 5(a)), while in $CoAs_2$-*Pnnm* and $CoAs_3$-*C*2/*m*, there exist strong hybridization between Co-d and As-p states (−2 to 2 eV). In $CoAs_2$ and $CoAs_3$, the pressure-induced transition from non-metal to metal was recognized. As is shown in ESI Fig. 5,† compared with the typical arsenide GaAs under the high pressure, all the novel phases of high pressure exhibit similar metallic properties. Due to the pressure, the electrons become unlocalized, making the material exhibit metallic properties.

It is worth noting that the electronic topological transition has a significant impact on the corresponding physical and chemical properties and can occur when the Fermi surface of the electronic system is changed by doping, high pressure, temperature or other external reagents.[44–46] Therefore, we have checked the potential pressure-induced electronic topological transition in Co–As system. Attractively, the electronic

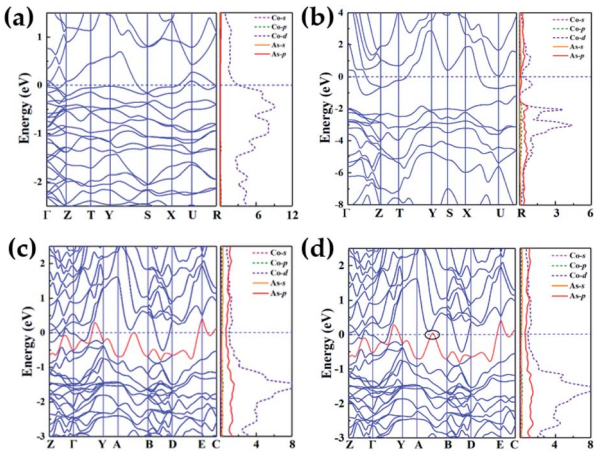

Fig. 5 Electronic band structure and the projected electronic DOS on Co atoms and As atoms for (a) Co_2As-*Pnma* at 1.28 GPa; (b) $CoAs_2$-*Pnnm* at 74.5 GPa; (c) $CoAs_3$-*C*2/*m* at 45.7 GPa, and (d) $CoAs_3$-*C*2/*m* at 48 GPa. Note that Zero energy is at the Fermi level.

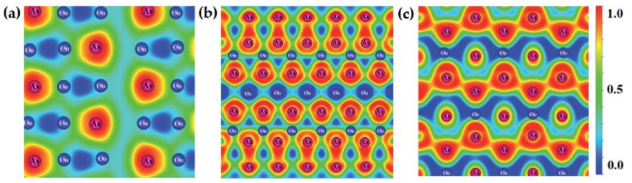

Fig. 6 Contours of the ELF for the structures of (a) Co_2As-*Pnma* at 1.28 GPa; (b) $CoAs_2$-*Pnnm* at 74.5 GPa, and (c) $CoAs_3$-*C*2/*m* at 45.7 GPa with isosurface of 0.8.

topological transition exists in $CoAs_3$-*C*2/*m* as shown in Fig. 5(c), it is found that there is no band along the A–B direction at 45.7 GPa. The band moves down and approaches to Fermi level at A–B direction when pressure increases. Fig. 5(d) clearly shows that the red band along the A–B direction is not fully occupied at 48 GPa and will form a hole pocket near the Fermi surface. An electronic topological transition in $CoAs_3$-*C*2/*m* structure is clearly observed since the noteworthy changes in the surface pro files Fermi at high pressure.

The electron localization function (ELF),[47] as depicted in Fig. 6, is used to understand bonding character of the Co–As compounds. Generally speaking, the regions with higher tendency of electron pairing (such as cores, and lone pairs) have large ELF values (>0.5), which indicates the formation of covalent bonds. However, the non/less electron localization have small values (<0.5), which indicates that there are ionic/metallic bonds between atoms. There is a mixed behaviour of ionic and metallic bonds simultaneously exits in Co_2As-*Pnma* phases. Note that in Fig. 6(b) and (c), the great ELF values about 0.8 between the Co and As atoms in $CoAs_2$-*Pnnm* and $CoAs_3$-*C*2/*m* structures, which suggests the covalent bonding character. The above statement is in good agreement with DOS. The DOS shows a large overlap between 3d states of Co and 4p states of As (Fig. 5(b) and (c)). Interestingly, in $CoAs_2$-*Pnnm* and $CoAs_3$-*C*2/*m* structure, it can be observed that there is electronic localization between As and As that does not favour either side, indicating the existence of nonpolar covalent bonds. It is more obvious that As atoms exist in chain form in $CoAs_3$-*C*2/*m*. To quantify the amount of charge belonging to each atom at different stoichiometries, we use the Bader charge analysis, which offers a description of electron transfer.[47]

4 Conclusions

In summary, three novel stable compounds (Co_2As-*Pnma*, $CoAs_2$-*Pnnm*, and $CoAs_3$-*C*2/*m*) of Co-As compounds are discovered under high pressure using unbiased structure searching combined with density functional theory calculations. The theoretical phonon dispersion curves suggest that all these phases are dynamically stable. The calculated electronic band structures and density of states suggest that the Co_2As-*Pnma*, $CoAs_2$-*Pnnm*, and $CoAs_3$-*C*2/*m* phases are metallic. Moreover, with the increase of pressure, the $CoAs_2$ and the $CoAs_3$ realize the transition from semiconductor to metal at 74.5 GPa and 45.7 GPa, respectively. A pressure-induced electronic topological transition has been found in $CoAs_3$-*C*2/*m* phase. The electron localization function results show that there are ionic bonds and metal bonds in the predicted structures. Further analysis of the bonding nature shows that, there are polar covalent bonds between Co atoms and As atoms in $CoAs_2$-*Pnnm*, and $CoAs_3$-*C*2/*m*. Our results are important for understanding the structures and properties of Co–As system under high pressure.

Author contributions

Conceptualization, A. Z., H. L.; methodology, S. L., Y. D., Y. H. and A. Z.; validation, A. Z., J. Y. and J. L.; writing—original draft, A. Z.; writing—review and editing, A. Z., Y. L. and T. C. All authors have read and agreed to the published version of the manuscript.

Conflicts of interest

There are no conflicts to declare.

Acknowledgements

The authors thank the financial support from the Natural Science Foundation of China (Grant No. 11764043).

Notes and references

1 Y. Ma, M. Eremets, A. R. Oganov, *et al.*, *Nature*, 2009, **458**(7235), 182–185.
2 M. Miao, *Nat. Chem.*, 2013, **5**(10), 846–852.
3 Y. Liu, R. Wang, Z. Wang, *et al.*, *Nat. Commun.*, 2022, **13**(1), 1–7.
4 N. N. Patel, A. K. Verma, A. K. Mishra, *et al.*, *Phys. Chem. Chem. Phys.*, 2017, **19**(11), 7996–8007.
5 Q. Zeng, S. Yu, D. Li, *et al.*, *Phys. Chem. Chem. Phys.*, 2017, **19**(12), 8236–8242.
6 J. Shi, W. Cui, J. A. Flores-Livas, *et al.*, *Phys. Chem. Chem. Phys.*, 2016, **18**(11), 8108–8114.
7 Y. Liu, C. Wang, P. Lv, H. Sun and D. Duan, *Chem.–Eur. J.*, 2018, **24**, 11402–11406.
8 X. Ma, X. Li, D. Zhou, J. Xu, W. Gao and Y. Liu, *J. Alloys Compd.*, 2019, **791**, 1257–1262.
9 M. Jacobsen, S. Sinogeikin, R. Kumar and A. Cornelius, *J. Phys. Chem. Solids*, 2012, **73**, 1154–1158.
10 S. V. Ovsyannikov and V. V. Shchennikov, *Chem. Mater.*, 2010, **22**, 635–647.
11 Y. Zhang, Y. Ma, A. Geng, C. Zhu, G. Liu, Q. Tao, F. Li, Q. Wang, Y. Li, X. Wang, *et al.*, *J. Alloys Compd.*, 2016, **685**, 551–558.
12 E. Uykur, R. Sankar, D. Schmitz and C. A. Kuntscher, *Phys. Rev. B*, 2018, **97**, 195134.
13 E. J. Cheng, W. Xia, X. B. Shi, Z. H. Yu, L. Wang, L. M. Yan, D. C. Peets, C. C. Zhu, H. Su, Y. Zhang, D. Z. Dai, X. Wang, Z. Q. Zou, N. Yu, X. F. Kou, W. W. Zhao, Y. F. Gao and S. Y. Li, *npj Quantum Mater.*, 2020, **5**, 38–45.
14 N. K. Ravichandran and D. Broido, *Nat. Commun.*, 2019, **10**, 1–8.

15 L. Wang, F. Tian, X. Liang, Y. Fu, X. Mu, J. Sun, X.-F. Zhou, K. Luo, Y. Zhang, Z. Zhao, *et al.*, *Phys. Rev. B*, 2019, **99**, 174104.
16 Y. Wang, J. Lv, L. Zhu and Y. Ma, *Comput. Phys. Commun.*, 2012, **183**, 2063–2070.
17 H. Wang, Y. Wang, J. Lv, Q. Li, L. Zhang and Y. Ma, *Comput. Mater. Sci.*, 2016, **112**, 406–415.
18 Y. Wang, J. Lv, L. Zhu and Y. Ma, *Phys. Rev. B*, 2010, **82**, 094116.
19 J. P. Perdew, K. Burke and M. Ernzerhof, *Phys. Rev. Lett.*, 1996, **77**, 3865.
20 G. Kresse and J. Furthmüller, *Phys. Rev. B*, 1996, **54**, 11169.
21 P. E. Blöchl, *Phys. Rev. B*, 1994, **50**, 17953.
22 D. Thirumalai, R. W. Hall and B. Berne, *J. Chem. Phys.*, 1984, **81**, 2523–2527.
23 H. J. Monkhorst and J. D. Pack, *Phys. Rev. B*, 1976, **13**, 5188.
24 P. Blaha, K. Schwarz, P. Sorantin and S. B. Trickey, *Comput. Phys. Commun.*, 1990, **59**, 399.
25 A. D. Becke and K. E. Edgecombe, *J. Chem. Phys.*, 1990, **92**, 5397–5403.
26 A. Togo, F. Oba and I. Tanaka, *Phys. Rev. B*, 2008, **78**, 134106.
27 K. Parlinski, Z. Li and Y. Kawazoe, *Phys. Rev. Lett.*, 1997, **78**, 4063.
28 P. S. Lyman and C. Prewitt, *Acta Crystallogr., Sect. B: Struct. Sci.*, 1984, **40**, 14–20.
29 J. C. Quesnel and R. Heyding, *Can. J. Chem.*, 1962, **40**, 814–818.
30 J. Ackermann and A. Wold, *J. Phys. Chem. Solids*, 1977, **38**, 1013–1016.
31 I. Lindeberg and Y. Andersson, *J. Alloys Compd.*, 1991, **175**, 163–169.
32 Q. Zhu, D. Y. Jung, A. R. Oganov, *et al.*, *Nat. Chem.*, 2013, **5**(1), 61–65.
33 X. Dong, A. R. Oganov, A. F. Goncharov, *et al.*, *Nat. Chem.*, 2017, **9**(5), 440–445.
34 S. Wei, D. Li, Y. Lv, Z. Liu, C. Xu, F. Tian, D. Duan, B. Liu and T. Cui, *Phys. Chem. Chem. Phys.*, 2016, **18**, 18074–18080.
35 X. Ren, X. Yan, Z. Yu, W. Li and L. Wang, *J. Alloys Compd.*, 2017, **725**, 941–945.
36 C. Xu, H. Yu, B. Kuo, S. Ma, X. Xiao, D. Li, D. Duan, X. Jin, B. Liu and T. Cui, *Phys. Chem. Chem. Phys.*, 2018, **20**, 6108–6115.
37 Y. Pan, W. Guan and Y. Li, *Phys. Chem. Chem. Phys.*, 2018, **20**, 15863–15870.
38 Y. Pan, *J. Alloys Compd.*, 2019, **779**, 813–820.
39 Y. Pan, P. Wang and C.-M. Zhang, *Ceram. Int.*, 2018, **44**, 12357–12362.
40 Y. Pan and W. Guan, *Phys. Chem. Chem. Phys.*, 2017, **19**, 19427–19433.
41 Y. Pan, *Mater. Res. Bull.*, 2017, **93**, 56–62.
42 H. Huang, H. H. Wu, C. Chi, J. Zhu, B. Huang and T. Y. Zhang, *Nanoscale*, 2019, **11**(40), 18758–18768.
43 H. H. Wu, H. Huang, J. Zhong, S. Yu, Q. Zhang and X. C. Zeng, *Nanoscale*, 2019, **11**(25), 12210–12219.
44 H. Ghosh and S. Sen, *J. Alloys Compd.*, 2016, **677**, 245–251.
45 Y. Zhang, L. Song, X. Shao, Y. Li, P. Zhu, H. Xu and J. Yang, *J. Alloys Compd.*, 2017, **715**, 237–241.
46 Y. Zhang, X. Shao, Y. Zheng, L. Yan, P. Zhu, Y. Li and H. Xu, *J. Alloys Compd.*, 2018, **732**, 280–285.
47 D. Song, D. Wan, H. H. Wu, D. Xue, S. Ning, M. Wu, T. Venkatesan and S. J. Pennycook, *Nanoscale*, 2020, **12**(12), 6844–6851.